NANO LETTERS

Letter

pubs.acs.org/NanoLett

Hierarchical Nanowire Arrays as Three-Dimensional Fractal Nanobiointerfaces for High Efficient Capture of Cancer Cells

Feilong Zhang,[†,§] Yan Jiang,[†,§] Xueli Liu,[†,§] Jingxin Meng,[‡] Pengchao Zhang,[†,§] Hongliang Liu,[‡] Gao Yang,[†,§] Guannan Li,[†,§] Lei Jiang,[‡,§] Li-Jun Wan,[†,§] Jin-Song Hu,*[,†,§] and Shutao Wang*[,‡,§]

[†]Beijing National Laboratory for Molecular Sciences (BNLMS), Institute of Chemistry, Chinese Academy of Sciences, Beijing 100190, P. R. China

[‡]Laboratory of Bio-inspired Smart Interface Science, CAS Center for Excellence in Nanoscience, Technical Institute of Physics and Chemistry, Chinese Academy of Sciences, Beijing 100190, P. R. China

[§]University of Chinese Academy of Sciences, Beijing 100049, P. R. China

S *Supporting Information*

ABSTRACT: A hierarchical assembled ITO nanowire array with both horizontal and vertical nanowire branches was fabricated as a new three-dimensional fractal nanobiointerface for efficient cancer cell capture. Comparing with ITO nanowire array without branches, this fractal nanobiointerface exhibited much higher efficiency (89% vs 67%) and specificity in capturing cancer cells and took shorter time (35 vs 45 min) to reach the maximal capture efficiency. As indicated by the immunofluorescent and ESEM images, this enhancement can be attributed to the improvement of topographical interaction between cells and the substrate. The introduction of horizontal and vertical nanowire branches makes the substrate topographically match better with cell filopodia and provides more binding sites for cell capture. The live/dead cell staining and proliferation experiments confirm that this fractal nanobiointerface displays excellent cyto-compatibility with an over 96% cell viability after capture. These results provide new insights and may open up opportunities in designing and engineering new cell-material interfaces for advanced biomedical applications.

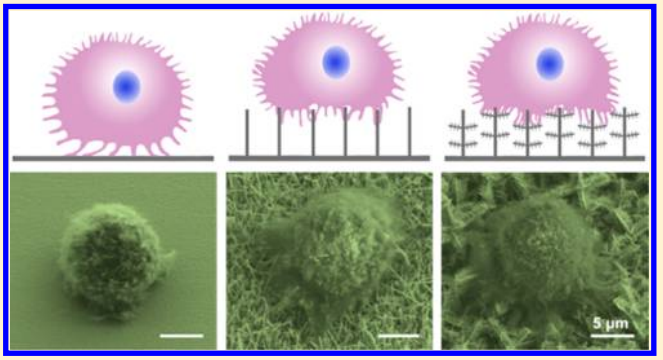

KEYWORDS: *Nanobiointerfaces, nanostructures, cell capture, topographical interaction, cyto-compatibility*

Three-dimensional (3D) nanobiointerface as a significant platform to guide cell fate has been emerging as a research focus in recent years.[1] Considering the microenvironments that cells inhabit including extracellular matrix (ECM) and special biomolecule, topographical,[2−7] mechanical,[8−14] and chemical factors[15−18] have been considered important in engineering cell biointerfaces. During the past years, a series of biointerfaces with the abilities to control cell adhesion/detachment[19,20] and differentiation,[6,21,22] help cell interconnect to outside,[23] or promote cell sensing to external signals[3,24] have been developed. These biointerfaces exhibit potentials in numerous biomedical applications, such as cell patterning,[25,26] drug/gene delivery,[27] and wound healing.[28]

Circulating tumor cells (CTCs), detaching from solid primary tumor and entering the bloodstream, have been regarded as a potentially accessible source for cancer diagnosis and monitoring. However, CTCs are extremely rare in the blood of patient (a few to hundreds per 10^9 hematologic cells), which brings a great challenge for CTCs detection.[29] Several types of microfluidic devices have been developed for CTCs isolation and achieved efficient and selective cell capture,[30−32] although they required complicated fabrication processes. Recently, researchers have revealed that macro/nanostructured surfaces modified with specific biomolecules could recognize and capture cancer cells with high efficiency and specificity.[33−47] Compared with a flat substrate, nanostructured substrates, including single vertical nanostructures, such as silicon nanopillars,[33] polystyrene (PS) nanotubes,[38] poly(3,4-ethylenedioxy) thiophene (PEDOTs) nanodots,[35] and single horizontal nanostructures, such as TiO_2,[37] poly(lactic-*co*-glycolic acid) (PLGA),[48] and PS nanofiber,[44] could achieve a higher capture efficiency of cancer cells. However, it is still of significant challenge to explore and engineer hierarchical biointerfaces with optimized structures to more efficiently recognize and detect rare cancer cells.

Here, we fabricated three types of ITO nanowire arrays, composed of single vertical nanowires, horizontal nanowire-branched nanowires, or horizontal and vertical nanowire-branched hierarchical nanowires, as 3D nanobiointerfaces for efficient cancer cell capture. The cancer cell-capture experi-

Received: November 19, 2015
Revised: December 10, 2015
Published: December 16, 2015

DOI: 10.1021/acs.nanolett.5b04731
Nano Lett. 2016, 16, 766−772

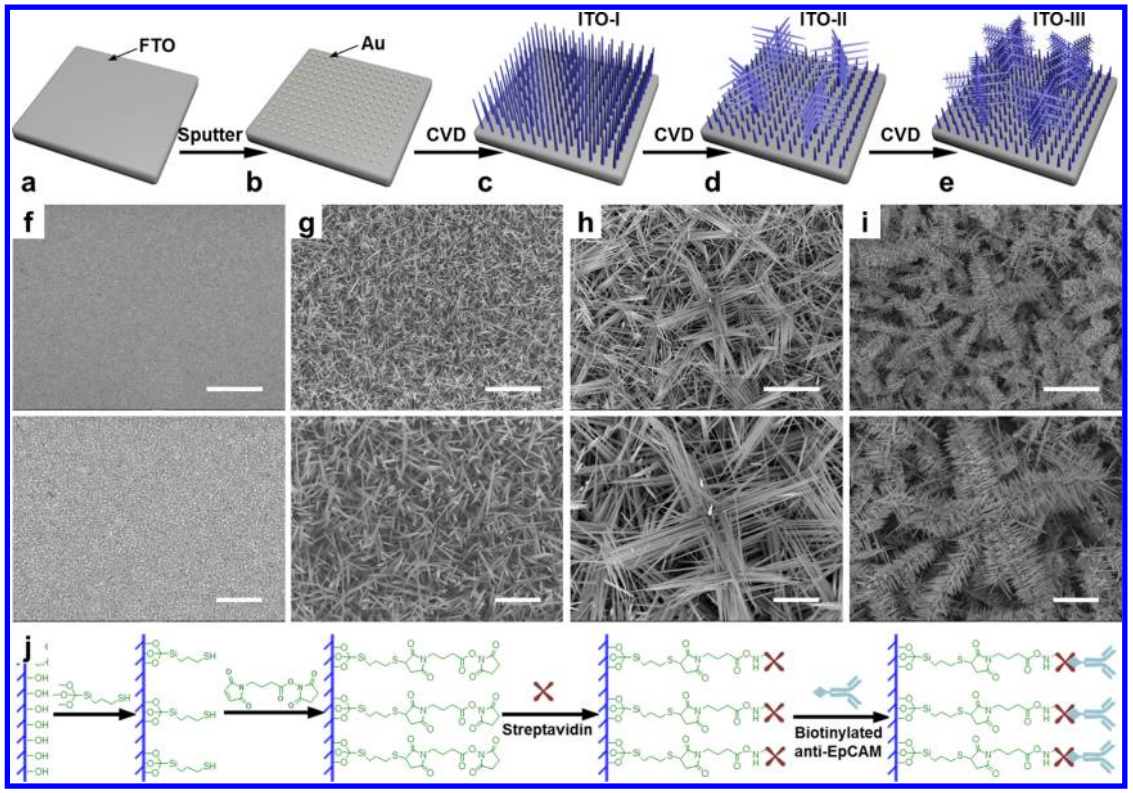

Figure 1. Fabrication and functionalization of hierarchical ITO nanowire arrays on FTO. (a–e) Schematic illustration of the fabrication of hierarchical ITO nanowire substrates. (a,b) The gold catalysts were deposited on the FTO substrates. (c–e) ITO-I, ITO-II, and ITO-III were step-by-step grown on substrate via CVD. (f–i) SEM images of a gold-sputtered FTO substrate, ITO-I, ITO-II, and ITO-III, respectively. Top: low-magnification images, scale bars are 5 μm. Bottom: high-magnification images, scale bars are 2 μm. (j) Illustration of the bioconjugation of epithelial cellular adhesion molecule antibody (anti-EpCAM) onto substrates to recognize and isolate target tumor cells specifically.

ments show that the nanowire array substrate significantly improved the cell-capture efficiency (67% vs 1.4%) in contrast to a flat substrate and the sensitivity to specific cell lines after the antibody modification as a result of the synergy between topographical effect and specific molecule recognition. Furthermore, the cell-capture efficiency and the sensitivity can be further enhanced by the introduction of branches on the nanowires. Compared with the substrate with single vertical nanowires, the hierarchical nanowire biointerfaces with both horizontal and vertical nanowire branches exhibited the best cell-capture efficiency (89% ± 6%) and specificity as well as a shortest time to reach the maximum of capture efficiency. This additional improvement can be attributed to the effects: (1) the horizontal nanowire branches topographically further enhanced the interaction of cell filopodia and materials; (2) the additional vertical branches on horizontal nanowire branches can further staple cells; and (3) all branches provided more binding sites on the substrate for cell capture. Moreover, the cell viability tests revealed that the developed 3D nanowire-based biointerfaces exhibited an excellent cyto-compatibility.

Results and Discussion. The hierarchical ITO nanowire arrays were fabricated via a multistep chemical vapor deposition (CVD) process (as illustrated Figure 1a–i).[49,50] Briefly, gold nanoparticles were sputtered as catalysts on an FTO substrate (Figure 1f) to grow the vertically aligned ITO nanowires with metallic indium and tin powers as sources (Figure 1a–c). The horizontal ITO nanowire branches were grown on the vertical ITO nanowires obtained in the first CVD step by repeating the above process (Figure 1c,d). The additional vertical ITO nanowire branches were subsequently grown on the above ITO nanowires with horizontal nanowire branches (Figure 1d,e). Then, these three kinds of ITO nanowire arrays were used as substrates for cell-capture experiments, denoted as ITO-I, ITO-II, and ITO-III, respectively. As shown in scanning electron microscope (SEM) image (Figure 1g), the nanowires on the ITO-I substrate were almost perpendicular to the FTO substrate giving a vertical structure (Figure 1g). Four rows of nanowire branches perpendicularly protruded from the four facets of the vertical nanowire stems on the ITO-II substrate to form horizontal nanowire branches (Figure 1h). On the ITO-III substrate, the additional short vertical nanowire branches were grown on the horizontal nanowire branches (Figure 1i). To achieve specific cancer cell capture, all three ITO nanowire substrates were modified with anti-EpCAM as a specific biomarker since EpCAM is a membrane antigen overexpressed in many cancer cell lines. After sequential chemical conjugation of 3-mercaptopropyl trimethoxysilane, *N*-maleimidobutyryloxy succinimide ester (GMBS), and streptavidin (SA), biotinylated anti-EpCAM can be grafted onto the substrates for the subsequent cell-capture experiments (Figure 1j).

To investigate the specific cell-capture performance of the anti-EpCAM-coated 3D ITO nanowire biointerfaces, EpCAM-positive cell lines (human breast cancer cell lines, MCF7, and human prostate cancer cell lines, PC3) and EpCAM-negative cells lines (cervical cancer cell lines, Hela) were chosen as target and control cell lines, respectively. To optimize the incubation time for optimal cell capture, a set of cell-capture experiments with different incubation times were first carried out using the anti-EpCAM-coated ITO nanowires arrays (ITO-I, ITO-II, and ITO-III) as substrates and MCF7 as target cells. The

DOI: 10.1021/acs.nanolett.5b04731
Nano Lett. 2016, 16, 766–772

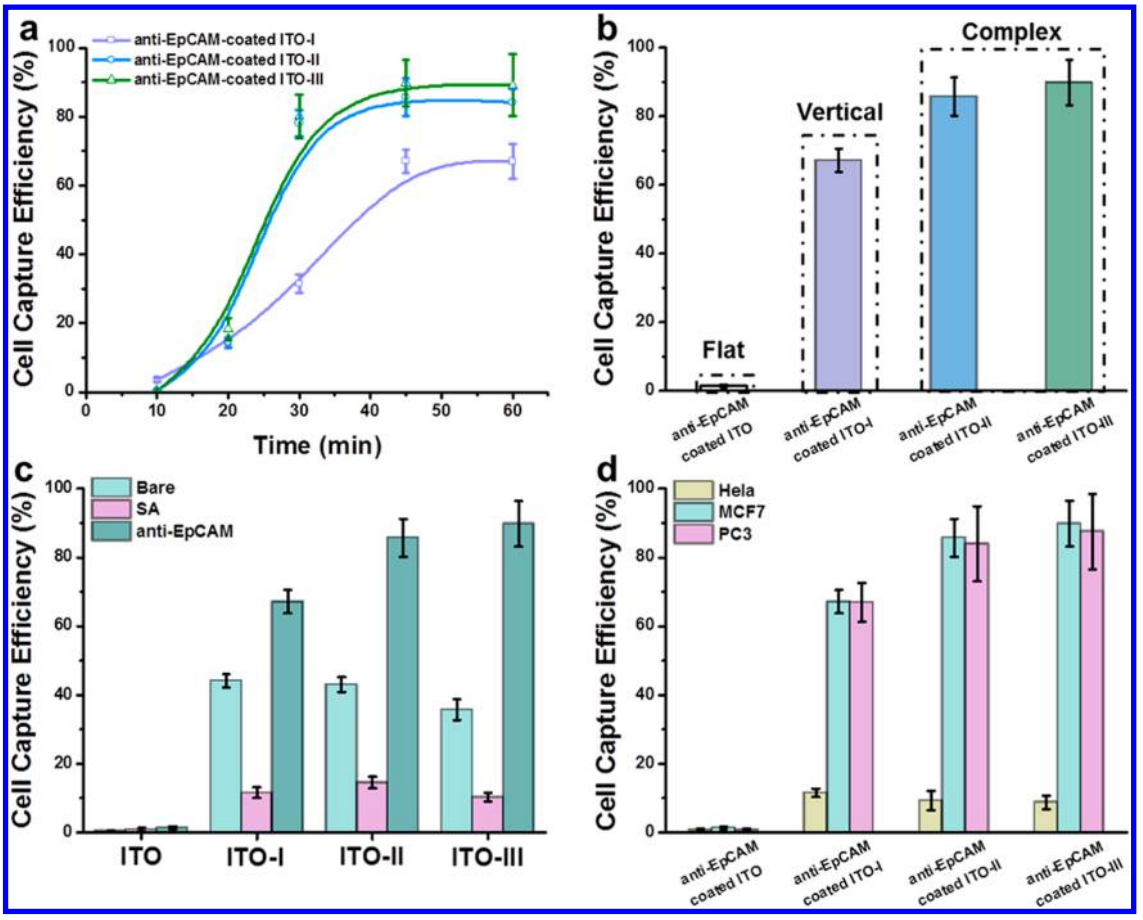

Figure 2. Quantitative evaluation of the cell-capture performance on different ITO nanobiointerfaces. (a) The cell-capture efficiencies of the anti-EpCAM-coated ITO nanobiointerfaces (ITO-I, ITO-II, and ITO-III) at various incubation times for MCF7 cells. (b) The cell-capture efficiencies of MCF7 cells on the anti-EpCAM coated flat ITO and ITO nanobiointerface. The flat ITO displayed a very low capture efficiency. The ITO-I nanobiointerfaces showed a capture efficiency of more than 60%. The ITO-II and ITO-III nanobiointerfaces gave an extra 18% and 22% of capture efficiency compared to that of ITO-I, respectively. (c) The influence of modified molecules (bare, SA, and anti-EpCAM) on the MCF7 cell-capture efficiency. The introduction of SA significantly reduced the nonspecific cell adhesion. The modification with anti-EpCAM gave a 70% more of capture efficiency compared with that of the SA-coated ITO-III substrate. (d) Cell-capture efficiencies of various cell lines (EpCAM-positive cells: MCF7, PC3. EpCAM-negative cells: Hela) on the anti-EpCAM-coated flat ITO and ITO nanobiointerfaces.

correlations between incubation time and the cell-capture efficiency (defined in the experimental section) of ITO substrates were plotted in Figure 2a. The maximal cell-capture efficiency was reached after 45 min incubation on the ITO-I substrate, which was similar to that on silicon-nanopillar (SiNP) substrate due to their similar topological morphology.[33] While the maximal cell-capture efficiencies were achieved at an incubation time of about 35 min on the ITO-II and ITO-III biointerfaces, which indicated that the hierarchical nano-biointerfaces with nanowire branches provided possibilities for rapid cancer diagnosis. In order to achieve the consistent comparison, 45 min was chosen as the incubation time in the subsequent experiments of cancer cell capture.

The cell-capture efficiencies of the four types of anti-EpCAM coated biointerfaces (flat ITO, ITO-I, ITO-II, and ITO-III) were determined after 45 min incubation to explore the effect of the substrate morphologies on the performance of cancer cell capture, which are 1.4% ± 0.4%, 67% ± 3%, 85% ± 5%, and 89% ± 6%, respectively (Figure 2b). Compared with the flat substrate, the nanostructures significantly enhanced the cell-capture efficiency. The ITO-I substrate gave the cell-capture efficiencies similar to Si nanopillar array substrate with similar single vertical structure (60−70%) (Figure S1), while an extra ∼18% of the cell-capture efficiency was achieved on ITO-II substrate and extra ∼22% on the ITO-III substrate. This enhancement can be attributed to that horizontal nanowire branches could form interfaces matching better with the cells, and the additional vertical branches on horizontal nanowire branches can further improve the cell−materials interfaces and staple cells.

To investigate the contribution of the modified biomolecules to the cell capture, we tested the cell-capture performance on the bare, SA-coated, and anti-EpCAM-coated substrates (each includes four types of substrates: flat ITO and three ITO nanobiointerfaces). The bare ITO nanobiointerfaces exhibited rather high nonspecific cell adhesion for MCF7 cells (Figure 2c), which may be related to the intrinsic nature of ITO. While, the introduction of SA brought a distinct reduction of the nonspecific cell adhesion. Furthermore, the conjugated anti-EpCAM improved the cell-capture efficiency up to 89% ± 6% (ITO-III nanobiointerface) corresponding to ∼80% enhancement compared with the SA-coated ITO-III nanobiointerface. These results revealed that the biomolecule (anti-EpCAM) significantly promoted the specific cell capture. To further explore the specificity of the anti-EpCAM-coated ITO nanobiointerfaces in cell capture, another EpCAM positive

DOI: 10.1021/acs.nanolett.5b04731
Nano Lett. 2016, 16, 766−772

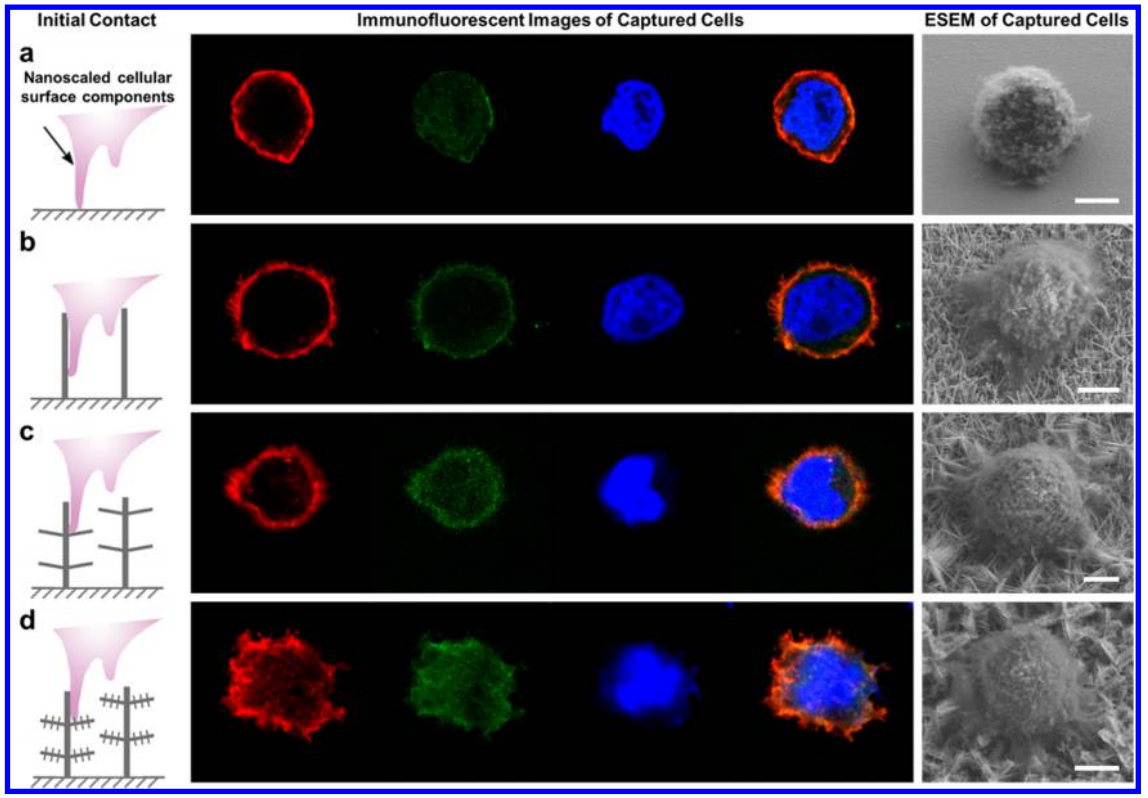

Figure 3. Comparison of the topographical interaction between MCF7 cells and the anti-EpCAM-modified substrates. (a–d) Typical morphologies of captured MCF7 cells on (a) flat FTO biointerface, (b) ITO-I biointerface, (c) ITO-II biointerface, and (d) ITO-III biointerface, respectively: scheme of initial contact state of cell and substrates (left), immunofluorescent images (middle), and ESEM images (right). Cells spread on the flat FTO substrate without obvious topographical interaction, while cells protruded lots of filopodia to match the nanostructures on nanowire array substrates (ITO-I, ITO-II, and ITO-III). The captured cells were costained for actin cytoskeleton (TRITC, red), focal adhesions (FITC, green), and nuclei (DAPI, blue) in the fluorescent images. All scale bars in SEM images are 5 μm.

cell line (PC3) and EpCAM-negative cell lines (Hela) were used to conduct cell-capture experiments. The PC3 cells displayed similar cell-capture efficiencies to that of MCF7 cells on all four kinds of substrates (flat ITO, ITO-I, ITO-II, and ITO-III) since they are both EpCAM positive cell lines. While the EpCAM-negative cells (Hela) exhibited very low nonspecific cell adhesion. Therefore, the modified biomolecule, anti-EpCAM, endowed the prepared biointerface with the enhancement of both efficiency and specificity in cancer cell capture.

The morphologies and cytoskeletons of cells captured on anti-EpCAM-coated different substrates were then investigated by environment scanning electron microscopy (ESEM) and immunofluorescent staining (Figure 3) to understand and explore the enhancement mechanism of the ITO nanobiointerfaces in cell-capture efficiency. After 45 min incubation, the MCF7 cells on the anti-EpCAM-coated flat ITO substrate remained spherical with few filopodia (Figure 3a), indicating a weak interaction between cells and substrate. In contrast, MCF7 cells on the ITO nanobiointerfaces (ITO-I, ITO-II, and ITO-III) protruded an amount of filopodia. This means that the cells interacted intimately with the nanobiointerface, resulting in the high cell-capture efficiency (about 60% enhancement compared with the flat ITO substrate). These results are consistent with the previously reported topographical interaction between cancer cells and nanostructures.[33] More interestingly, it was observed from the ESEM and fluorescent images that the filopodia of cells on the complex ITO nanobiointerfaces (ITO-II and ITO-III) protruded along the horizontal ITO nanowire branches, which increased the contact area and interaction between filopodia and substrate. This improved interaction contributed to the 20% enhancement of cell-capture efficiency against that of the ITO-I nanobiointerface. What's more, the cells on ITO-III biointerface exhibited the largest amount of filopodia, which may be owing to the pinning effect of the vertical nanowire branches on horizontal branches. Therefore, the hierarchical nanowire structures with both horizontal and vertical nanowire branches exhibited the best intimate matching with cancer cells and enhanced the topographical interaction between cells and substrate, resulting in the improvement of cell-capture efficiency compared with the substrate with vertical nanowires alone without branches.

In addition, the cyto-compatibility of the ITO nanobiointerface was assessed to guarantee the subsequent cell culture and biological studies after cell capture. First, the viability of cells before and after the capture on the ITO-III nanobiointerface was determined via the live/dead cell staining with acridine orange/propidium iodide (AO/PI) dyes (Figure 4a,b). As shown in Figure 4b, the viability of the captured cells reached up to 96.4%. Second, we conducted a continuous culture of the cells captured on the ITO-III nanobiointerface after the cell-capture experiment. The cells exhibited good spreading and proliferation behavior in a long-term incubation. As shown in Figure 4c, the cells captured on the ITO-III nanobiointerface spread gradually with incubation (12 to 24 h) and apparently proliferated after 48 h incubation. The cell coverage was introduced to evaluate the cell behaviors of spreading and

DOI: 10.1021/acs.nanolett.5b04731
Nano Lett. 2016, 16, 766–772

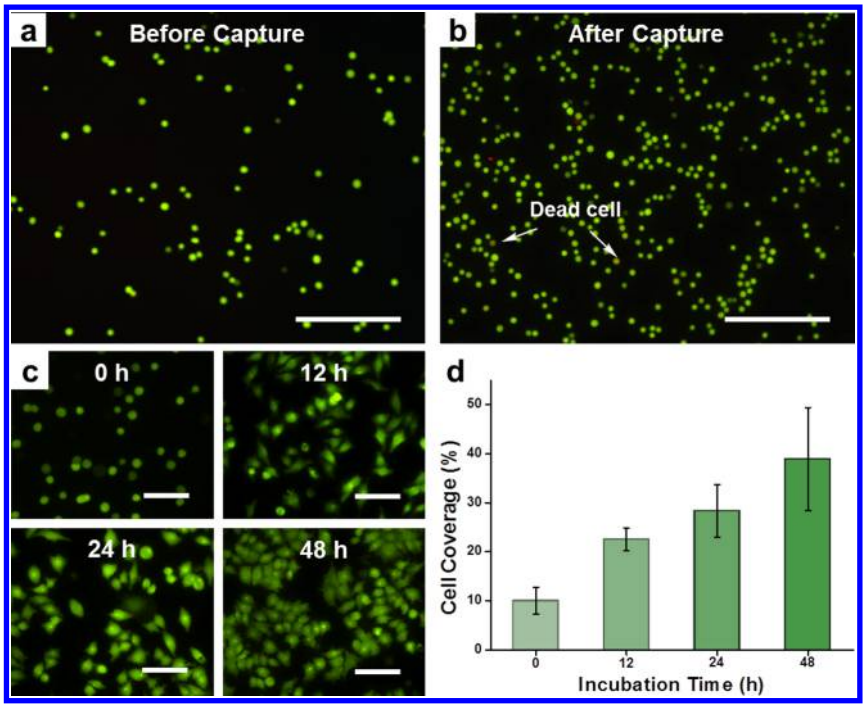

Figure 4. Cyto-compatibility test of the ITO nanobiointerfaces. (a) Fluorescent images of MCF7 cell suspension before capture experiments and (b) stained MCF7 cells captured on anti-EpCAM-modified ITO-III biointerface. Cell viability test was conducted by staining with acridine orange/propidium iodite (AO/PI). The viable cells were only stained in green by AO, while the dead cells were stained in green + red by AO and PI. Scale bars are 200 μm. (c) Fluorescent images of MCF7 cells captured on anti-EpCAM-modified ITO-III biointerface after incubation for 0, 12, 24, and 48 h, respectively. Scale bars are 100 μm. (d) The cell coverage as a function of incubation time.

proliferation. The statistical results in Figure 4d showed that the cell coverage increased from 10.0% ± 2.7% to 22.5% ± 2.3%, 28.3% ± 5.4% and 38.9% ± 10.5% after 12, 24, and 48 h incubation, respectively, indicating the excellent cyto-compatibility of the ITO nanobiointerfaces.

Conclusions. In summary, we have fabricated a hierarchical three-dimensional ITO nanobiointerface, which consists of vertical nanowire array with horizontal and vertical nanowire branches. This hierarchical nanobiointerface exhibited extremely high efficiency and specificity in cancer cell capture when coated with cell-capture agent in virtue of the synergy between the molecule recognition and topographical interaction. Compared with the nanobiointerface with vertical nanowires alone, the introduction of horizontal and vertical nanowire branches in the fractal nanobiointerface significantly enhanced the cell-capture efficiency and shortened the incubation time to reach the maximal cell-capture efficiency. This enhancement can be ascribed to the improvement of topographical interaction arising from the more closely matching of the structures with cancer cells. The ITO nanobiointerface is also of excellent cyto-compatibility, which is conducive to the following cell culture and biological studies. These results provide new clues and may open up opportunities in designing and engineering new biointerfaces for biological applications by harnessing the synergy between vertical and horizontal structures.

Experimental Section. *Preparation of 3D ITO Nanowire Substrates.* The 3D ITO nanowire substrates were fabricated by a multistep chemical vapor deposition process. First, FTO substrates (14 Ω/□, Nippon Sheet Glass) were cleaned by sequentially sonicating in water, ethanol, and acetone thoroughly, followed by O_2 plasma cleaning for subsequent use. Then, gold nanoparticles were sputtered on the FTO as catalysts via a sputtering coater. The first-generation ITO nanowire arrays (ITO-I) were fabricated by first CVD step with high-purity metallic indium and tin powders (m/m = 10:1) as source at a source temperature of 800 °C, a pressure of 30 Pa, and an air flow of about 1.5 sccm. The horizontal nanowire branches were grown on ITO-I nanowire arrays by repeating the above procedure to get ITO-II, followed by the growth of the additional branches via similar process to achieve ITO-III.

Surface Modification with Streptavidin (SA). The substrates were immersed in 4% (v/v) 3-mercaptopropyl trimethoxysilane in ethanol at room temperature overnight after treated with oxygen plasma at 200 W for 300 s. After three times of rinsing with ethanol and subsequent dimethyl sulfoxide (DMSO), the coupling agent GMBS was attached on the substrate by immersing in GMBS solution (0.25×10^{-3} M in DMSO) for 30 min. Then, the substrates were treated with 10 μg mL^{-1} of SA at room temperature for 45 min to graft SA onto GMBS and then rinsed more than 3 times with 1 × PBS to remove excess SA.

Cell-Capture Experiments. The cell-capture experiments were performed as described previously.[33] Before cell-capture experiments, a 1 cm × 1 cm substrate (immobilized with SA) was covered by 25 μL of biotinylated anti-EpCAM (10 μg mL^{-1} in PBS) and incubated for 30 min. The anti-EpCAM coated ITO nanowire array interfaces were placed into a commercial 6-well cell culture plate (generally 3 substrates in one well) and then loaded 3 mL of cell suspensions (10^5 cells mL^{-1}). After incubating 45 min at 37 °C and 5% CO_2, the ITO nanowire array interfaces were gently washed with PBS at least 5 times. The captured cells on the substrates were fixed with 4% PBS solution of paraformaldehyde (PFA) for 20 min. In order to induce cellular permeability and to allow for intracellular staining, the samples were treated with 0.2% Triton X-100 in

DOI: 10.1021/acs.nanolett.5b04731
Nano Lett. 2016, 16, 766−772

PBS for 10 min. To permit the identification of cellular nuclei, the ITO nanobiointerfaces were incubated with a DAPI solution (2 μg mL^{-1}) for 15 min, followed by three times of PBS washes. Then the substrates were placed onto a standard cover glass for fluorescent microscope observation. Finally, we imaged and counted cells using the fluorescence microscope (Nikon Ti-E).

The cell-capture efficiency was defined as the ratio of the experimental cell density captured on the substrate and the theoretical value. The number of captured cells was counted on a basis of a fluorescence image after cell-capture experiments. Nine fluorescence images were randomly taken on the different locations of a substrate to give an average cell number. The experimental cell density was defined by the average cell number on an image (n)/the image area (a). The theoretical cell density was the ratio of the total cell number (N) and the total bottom area of the cell culture plate (A). Then,

$$\text{cell-capture efficiency} = \frac{n/a}{N/A} \times 100\% = \frac{nA}{Na} \times 100\%$$

In our experiments, a was 0.011 cm^2; N was 3×10^5; and A was 9.6 cm^2, which will give:

$$\text{cell-capture efficiency} = \frac{nA}{Na} \times 100\% = \frac{n}{344} \times 100\%$$

Three substrates were tested in parallel in each experiment to give an error bar for each cell-capture efficiency.

Cell Morphologies Observation. After the cell-capture experiments, the cells captured on the substrates were fixed with glutaraldehyde (2.5% in PBS) for more than 4 h at room temperature. Then, the substrates immersed in a series of alcohol aqueous solution with different volume fractions (0, 30%, 50%, 75%, 85%, 95%, and 100%) in sequence. After drying in carbon dioxide under supercritical condition, the cell morphology was checked with an ESEM (FEI 10 Quanta 200) operated at low vacuum (93 Pa).

Immunofluorescent Staining for Actin Cytoskeleton and Focal Adhesions (FAs) of Captured Cells. After 45 min of incubation, MCF7 cells captured on the anti-EpCAMmodified ITO substrates were immersed in 4% paraformaldehyde (in PBS) for 20 min followed by three times of washing with PBS, 0.2% Triton-X100 (in PBS) for 5 min to increase the cell permeability (with a following three times of washing), and then 2% BSA (in PBS) for 30 min at RT, in sequence. After removing the block solutions (without washing), the substrate surfaces were covered with the primary antibody (antivinculin mouse monoclonal, diluted 1:400, 50 μL per 1 cm × 1 cm substrate) for 1 h (RT). After washing with PBS three times, cells were incubated with the secondary antibody (FITC-conjugated goat antimouse, diluted 1:30) for 30 min (RT). Then, the actin cytoskeleton was stained using TRITC-conjugated Phalloidin (15 mg in 250 mL of methanol and diluted 1:100 using 2% BSA) for 30 min (RT). After washing with PBS three times, cells were stained with DAPI (2 μg mL^{-1}) for 5 min. After three times washing, the samples were stored in dark in PBS (4 °C) for the subsequent observation with a confocal laser scanning biological microscope FV1000-LX81 (Olympus, Japan).

Cell Viability Assay. The cell viability of MCF7 cells before and after the capture on the ITO-III nanobiointerface was investigated using Live/Dead staining method with acridine orange/propidium iodide (AO/PI) dyes. The AO/PI working solution was prepared by mixing 0.5 μg/mL AO solution and 0.5 μg mL^{-1} PI solution at the volume ratio of 1:1. For the cell suspension before cell-capture experiment, the cells were stained by adding AO/PI working solution to the prepared cell suspension (10^6 mL^{-1}) (volume ratio: 5 μL mL^{-1}) for 15 min with shaking every 5 min. After staining, the stained cells were separated from the staining solution by centrifugation at 1000 rpm for 3 min. Then, the cells were washed with fresh DMEM medium for 3 times and dispersed with DMEM medium again. The cells captured on the ITO nanobiointerfaces were stained by adding 0.5 mL AO/PI working solution onto the substrate for 3 min. Then, we took images and evaluated the cell viability with fluorescent microscope.

Cell Proliferation Assay. To test the cyto-compatibility of the ITO-III nanobiointerfaces, the cells captured on the substrates were subjected to a long-term culture. In detail, after the cell-capture experiments, the substrates with the captured cells (MCF7 cells) were immersed in fresh DMEM medium for culture. After a certain time of incubation (12, 24, and 48 h), the cells were stained by calcein and checked with fluorescent microscope.

■ ASSOCIATED CONTENT

Supporting Information

The Supporting Information is available free of charge on the ACS Publications website at DOI: 10.1021/acs.nanolett.5b04731.

Detailed information about the materials used in this work and the comparison of cell-capture performance between ITO-I and SiNP substrates (PDF)

■ AUTHOR INFORMATION

Corresponding Authors

*E-mail: hujs@iccas.ac.cn.

*E-mail: stwang@mail.ipc.ac.cn.

Author Contributions

The first two authors contributed equally to this work.

Notes

The authors declare no competing financial interest.

■ ACKNOWLEDGMENTS

This research is supported by the National Research Fund for Fundamental Key Projects (2012CB933800) and National Natural Science Foundation (21175140, 21425314, 21421061, 21504098, 91127044, 21573249, and 21501184), 863 Program (2013AA032203), and MOST (2013YQ190467), and the Strategic Priority Research Program of the Chinese Academy of Sciences (XDB12020100).

■ REFERENCES

(1) Liu, X.; Wang, S. *Chem. Soc. Rev.* **2014**, *43*, 2385−2401.

(2) Chen, C. S.; Mrksich, M.; Huang, S.; Whitesides, G. M.; Ingber, D. E. *Science* **1997**, *276*, 1425−1428.

(3) Yang, M. T.; Sniadecki, N. J.; Chen, C. S. *Adv. Mater.* **2007**, *19*, 3119−3123.

(4) Bettinger, C. J.; Langer, R.; Borenstein, J. T. *Angew. Chem., Int. Ed.* **2009**, *48*, 5406−5415.

(5) Chen, A.; Lieu, D. K.; Freschauf, L.; Lew, V.; Sharma, H.; Wang, J.; Nguyen, D.; Karakikes, I.; Hajjar, R. J.; Gopinathan, A.; Botvinick, E.; Fowlkes, C. C.; Li, R. A.; Khine, M. *Adv. Mater.* **2011**, *23*, 5785−5791.

(6) Bucaro, M. A.; Vasquez, Y.; Hatton, B. D.; Aizenberg, J. *ACS Nano* **2012**, *6*, 6222−6230.

DOI: 10.1021/acs.nanolett.5b04731
Nano Lett. 2016, 16, 766−772

(7) Li, Y.-Q.; Zhu, B.; Li, Y.; Leow, W. R.; Goh, R.; Ma, B.; Fong, E.; Tang, M.; Chen, X. *Angew. Chem., Int. Ed.* **2014**, *53*, 5837−5841.
(8) Pelham, R. J.; Wang, Y.-l. *Proc. Natl. Acad. Sci. U. S. A.* **1997**, *94*, 13661−13665.
(9) Discher, D. E.; Janmey, P.; Wang, Y.-l. *Science* **2005**, *310*, 1139−1143.
(10) Engler, A. J.; Sen, S.; Sweeney, H. L.; Discher, D. E. *Cell* **2006**, *126*, 677−689.
(11) Vogel, V.; Sheetz, M. *Nat. Rev. Mol. Cell Biol.* **2006**, *7*, 265−275.
(12) Discher, D. E.; Mooney, D. J.; Zandstra, P. W. *Science* **2009**, *324*, 1673−1677.
(13) Fu, J.; Wang, Y.-K.; Yang, M. T.; Desai, R. A.; Yu, X.; Liu, Z.; Chen, C. S. *Nat. Methods* **2010**, *7*, 733−736.
(14) Trappmann, B.; Gautrot, J. E.; Connelly, J. T.; Strange, D. G. T.; Li, Y.; Oyen, M. L.; Cohen Stuart, M. A.; Boehm, H.; Li, B.; Vogel, V.; Spatz, J. P.; Watt, F. M.; Huck, W. T. S. *Nat. Mater.* **2012**, *11*, 642−649.
(15) Petersen, S.; Alonso, J. M.; Specht, A.; Duodu, P.; Goeldner, M.; del Campo, A. *Angew. Chem.* **2008**, *120*, 3236−3239.
(16) Melkoumian, Z.; Weber, J. L.; Weber, D. M.; Fadeev, A. G.; Zhou, Y.; Dolley-Sonneville, P.; Yang, J.; Qiu, L.; Priest, C. A.; Shogbon, C.; Martin, A. W.; Nelson, J.; West, P.; Beltzer, J. P.; Pal, S.; Brandenberger, R. *Nat. Biotechnol.* **2010**, *28*, 606−610.
(17) Zhang, Z.; Chen, N.; Li, S.; Battig, M. R.; Wang, Y. *J. Am. Chem. Soc.* **2012**, *134*, 15716−15719.
(18) Hu, B.; Shi, W.; Wu, Y.-L.; Leow, W. R.; Cai, P.; Li, S.; Chen, X. *Adv. Mater.* **2014**, *26*, 5786−5793.
(19) Liu, H.; Liu, X.; Meng, J.; Zhang, P.; Yang, G.; Su, B.; Sun, K.; Chen, L.; Han, D.; Wang, S.; Jiang, L. *Adv. Mater.* **2013**, *25*, 922−927.
(20) Liu, H.; Li, Y.; Sun, K.; Fan, J.; Zhang, P.; Meng, J.; Wang, S.; Jiang, L. *J. Am. Chem. Soc.* **2013**, *135*, 7603−7609.
(21) Namgung, S.; Baik, K. Y.; Park, J.; Hong, S. *ACS Nano* **2011**, *5*, 7383−7390.
(22) Park, J.; Bauer, S.; von der Mark, K.; Schmuki, P. *Nano Lett.* **2007**, *7*, 1686−1691.
(23) Kim, W.; Ng, J. K.; Kunitake, M. E.; Conklin, B. R.; Yang, P. *J. Am. Chem. Soc.* **2007**, *129*, 7228−7229.
(24) Teo, B. K. K.; Wong, S. T.; Lim, C. K.; Kung, T. Y. S.; Yap, C. H.; Ramagopal, Y.; Romer, L. H.; Yim, E. K. F. *ACS Nano* **2013**, *7*, 4785−4798.
(25) Lopez, G. P.; Albers, M. W.; Schreiber, S. L.; Carroll, R.; Peralta, E.; Whitesides, G. M. *J. Am. Chem. Soc.* **1993**, *115*, 5877−5878.
(26) Li, G.; Yang, G.; Zhang, P.; Li, Y.; Meng, J.; Liu, H.; Wang, S. *Small* **2015**, *11*, 5642−5646.
(27) Fischer, K. E.; Alemán, B. J.; Tao, S. L.; Daniels, R. H.; Li, E. M.; Bünger, M. D.; Nagaraj, G.; Singh, P.; Zettl, A.; Desai, T. A. *Nano Lett.* **2009**, *9*, 716−720.
(28) Xi, Y.; Dong, H.; Sun, K.; Liu, H.; Liu, R.; Qin, Y.; Hu, Z.; Zhao, Y.; Nie, F.; Wang, S. *ACS Appl. Mater. Interfaces* **2013**, *5*, 4821−4826.
(29) Steeg, P. S. *Nat. Med.* **2006**, *12*, 895−904.
(30) Nagrath, S.; Sequist, L. V.; Maheswaran, S.; Bell, D. W.; Irimia, D.; Ulkus, L.; Smith, M. R.; Kwak, E. L.; Digumarthy, S.; Muzikansky, A.; Ryan, P.; Balis, U. J.; Tompkins, R. G.; Haber, D. A.; Toner, M. *Nature* **2007**, *450*, 1235−1239.
(31) Stott, S. L.; Hsu, C.-H.; Tsukrov, D. I.; Yu, M.; Miyamoto, D. T.; Waltman, B. A.; Rothenberg, S. M.; Shah, A. M.; Smas, M. E.; Korir, G. K.; Floyd, F. P.; Gilman, A. J.; Lord, J. B.; Winokur, D.; Springer, S.; Irimia, D.; Nagrath, S.; Sequist, L. V.; Lee, R. J.; Isselbacher, K. J.; Maheswaran, S.; Haber, D. A.; Toner, M. *Proc. Natl. Acad. Sci. U. S. A.* **2010**, *107*, 18392−18397.
(32) Ozkumur, E.; Shah, A. M.; Ciciliano, J. C.; Emmink, B. L.; Miyamoto, D. T.; Brachtel, E.; Yu, M.; Chen, P.-i.; Morgan, B.; Trautwein, J.; Kimura, A.; Sengupta, S.; Stott, S. L.; Karabacak, N. M.; Barber, T. A.; Walsh, J. R.; Smith, K.; Spuhler, P. S.; Sullivan, J. P.; Lee, R. J.; Ting, D. T.; Luo, X.; Shaw, A. T.; Bardia, A.; Sequist, L. V.; Louis, D. N.; Maheswaran, S.; Kapur, R.; Haber, D. A.; Toner, M. *Sci. Transl. Med.* **2013**, *5*, 179ra47.
(33) Wang, S.; Wang, H.; Jiao, J.; Chen, K.-J.; Owens, G. E.; Kamei, K.-i.; Sun, J.; Sherman, D. J.; Behrenbruch, C. P.; Wu, H.; Tseng, H.-R. *Angew. Chem., Int. Ed.* **2009**, *48*, 8970−8973.
(34) Chen, L.; Liu, X.; Su, B.; Li, J.; Jiang, L.; Han, D.; Wang, S. *Adv. Mater.* **2011**, *23*, 4376−4380.
(35) Sekine, J.; Luo, S.-C.; Wang, S.; Zhu, B.; Tseng, H.-R.; Yu, H.-h. *Adv. Mater.* **2011**, *23*, 4788−4792.
(36) Wang, S.; Liu, K.; Liu, J.; Yu, Z. T. F.; Xu, X.; Zhao, L.; Lee, T.; Lee, E. K.; Reiss, J.; Lee, Y.-K.; Chung, L. W. K.; Huang, J.; Rettig, M.; Seligson, D.; Duraiswamy, K. N.; Shen, C. K. F.; Tseng, H.-R. *Angew. Chem., Int. Ed.* **2011**, *50*, 3084−3088.
(37) Zhang, N.; Deng, Y.; Tai, Q.; Cheng, B.; Zhao, L.; Shen, Q.; He, R.; Hong, L.; Liu, W.; Guo, S.; Liu, K.; Tseng, H.-R.; Xiong, B.; Zhao, X.-Z. *Adv. Mater.* **2012**, *24*, 2756−2760.
(38) Liu, X.; Chen, L.; Liu, H.; Yang, G.; Zhang, P.; Han, D.; Wang, S.; Jiang, L. *NPG Asia Mater.* **2013**, *5*, e63.
(39) Zhang, P.; Chen, L.; Xu, T.; Liu, H.; Liu, X.; Meng, J.; Yang, G.; Jiang, L.; Wang, S. *Adv. Mater.* **2013**, *25*, 3566−3570.
(40) Liu, X.; Zhang, F.; Wang, Q.; Gao, J.; Meng, J.; Wang, S.; Yang, Z.; Jiang, L. *Small* **2014**, *10*, 4677−4683.
(41) Meng, J.; Liu, H.; Liu, X.; Yang, G.; Zhang, P.; Wang, S.; Jiang, L. *Small* **2014**, *10*, 3735−3741.
(42) Yang, G.; Liu, H.; Liu, X.; Zhang, P.; Huang, C.; Xu, T.; Jiang, L.; Wang, S. *Adv. Healthcare Mater.* **2014**, *3*, 332−337.
(43) Li, Y.; Lu, Q.; Liu, H.; Wang, J.; Zhang, P.; Liang, H.; Jiang, L.; Wang, S. *Adv. Mater.* **2015**, *27*, 6848−6854.
(44) Ma, L.; Yang, G.; Wang, N.; Zhang, P.; Guo, F.; Meng, J.; Zhang, F.; Hu, Z.; Wang, S.; Zhao, Y. *Adv. Healthcare Mater.* **2015**, *4*, 838−843.
(45) Meng, J.; Zhang, P.; Zhang, F.; Liu, H.; Fan, J.; Liu, X.; Yang, G.; Jiang, L.; Wang, S. *ACS Nano* **2015**, *9*, 9284−9291.
(46) Yin, S.; Wu, Y.-L.; Hu, B.; Wang, Y.; Cai, P.; Tan, C. K.; Qi, D.; Zheng, L.; Leow, W. R.; Tan, N. S.; Wang, S.; Chen, X. *Adv. Mater. Interfaces* **2014**, *1*, 43.
(47) Li, Y.-Q.; Chandran, B. K.; Lim, C. T.; Chen, X. *Adv. Sci.* **2015**, *2*, 118.
(48) Hou, S.; Zhao, L.; Shen, Q.; Yu, J.; Ng, C.; Kong, X.; Wu, D.; Song, M.; Shi, X.; Xu, X.; OuYang, W.-H.; He, R.; Zhao, X.-Z.; Lee, T.; Brunicardi, F. C.; Garcia, M. A.; Ribas, A.; Lo, R. S.; Tseng, H.-R. *Angew. Chem., Int. Ed.* **2013**, *52*, 3379−3383.
(49) Jiang, Y.; Zhang, X.; Ge, Q.-Q.; Yu, B.-B.; Zou, Y.-G.; Jiang, W.-J.; Song, W.-G.; Wan, L.-J.; Hu, J.-S. *Nano Lett.* **2014**, *14*, 365−372.
(50) Jiang, Y.; Yu, B.-B.; Liu, J.; Li, Z.-H.; Sun, J.-K.; Zhong, X.-H.; Hu, J.-S.; Song, W.-G.; Wan, L.-J. *Nano Lett.* **2015**, *15*, 3088−3095.

DOI: 10.1021/acs.nanolett.5b04731
Nano Lett. 2016, 16, 766−772